This is a preprint, the final version is subject to change, of the American Mineralogist (MSA)
Cite as Authors (Year) Title. American Mineralogist, in press.
DOI: https://doi.org/10.2138/am-2020-7204

7204R2 – Revision 2

Incorporation of Mg in Phase Egg, $AlSiO_3OH$: Toward a new polymorph of Phase H, $MgSiH_2O_4$, a carrier of water in the deep mantle

LUCA BINDI[1,2,*], ALEKSANDRA BENDELIANI[3,4], ANDREY BOBROV[3,4,5], EKATERINA MATROSOVA[4], TETSUO IRIFUNE[6,7]

[1]Dipartimento di Scienze della Terra, Università degli Studi di Firenze,Via G. La Pira 4, I-50121 Firenze, Italy
[2]C.N.R., Istituto di Geoscienze e Georisorse, Sezione di Firenze, Via G. La Pira 4, I-50121 Firenze, Italy
[3]Geological Faculty, Moscow State University, Moscow 119991, Russia
[4]Vernadsky Institute of Geochemistry and Analytical Chemistry of Russian Academy of Sciences, Moscow 119991, Russia
[5]Korzhinskii Institute of Experimental Mineralogy, Chernogolovka, Moscow oblast 142432, Russia
[6]Geodynamics Research Center, Ehime University, Matsuyama 790-8577, Japan
[7]Earth-Life Science Institute, Tokyo Institute of Technology, Tokyo 152-8550, Japan

*Corresponding Author: luca.bindi@unifi.it

ABSTRACT

The crystal structure and chemical composition of a crystal of Mg-bearing Phase Egg with general formula $M^{3+}_{1-x}M^{2+}_{x}SiO_4H_{1+x}$ (M^{3+} = Al, Cr; M^{2+} = Mg, Fe), with x = 0.35, produced by subsolidus reaction at 24 GPa and 1400 °C of components of subducted oceanic slabs (peridotite, basalt, and sediment), was analyzed by electron microprobe and single-crystal X-ray diffraction. Neglecting the enlarged unit-cell and the consequent expansion of the coordination polyhedra (as expected for Mg substitution for Al), the compound was found to be topologically identical to Phase Egg, $AlSiO_3OH$, space group $P2_1/n$, with lattice parameters a = 7.2681(8), b = 4.3723(5), c = 7.1229(7) Å, β = 99.123(8)°, V = 223.49(4) Å^3, and Z = 4. Bond-valence considerations lead to hypothesize the presence of hydroxyl groups only, thus excluding the presence of the molecular water that would be present in hypothetical endmember $MgSiO_3 \cdot H_2O$. We thus demonstrate that Phase Egg, considered as one of the main players in the water cycle of the mantle, can incorporate large amounts of Mg in its structure and that there exists a solid solution with a

new hypothetical $MgSiH_2O_4$ endmember, according to the reaction $Al^{3+} \Leftrightarrow Mg^{2+} + H^+$. The new hypothetical $MgSiH_2O_4$ endmember would be a polymorph of Phase H, a leading candidate for delivering significant water to the deepest part of the lower mantle.

Keywords: Phase Egg; Phase H; hydrous dense magnesium silicate; synthesis; microprobe analysis; X-ray diffraction; crystal structure.

INTRODUCTION

Transportation of water into the Earth's deep interior by the subduction of oceanic slabs plays a key role in the geodynamics of our planet through its impact on the rheology and electrical conductivity of the mantle (e.g., Ohtani et al. 2000; Ohira et al. 2014). Broad experimental stability field have been reported for Al-bearing hydrous phases and dense hydrous magnesium silicates, leading to wide agreement that these are the main players in the water cycle of the mantle (Frost and Fei 1998; Shieh et al. 1998; Tsuchiya 2013; Nishi et al. 2014; Pamato et al. 2015). Among these compounds, Phase Egg, $AlSiO_3OH$ (Eggleton et al. 1978; Schmidt et al. 1998; Fukuyama et al. 2017), likely found as inclusion in natural diamonds (Wirth et al. 2007; Kaminsky 2012), is considered to be the most promising candidate water carrier in ringwoodite-free lithologies in the lower half of the mantle transition zone, which is now established to be hydrous also by direct evidence obtained through natural samples (Pearson et al. 2014; Smith et al. 2016, 2018).

Although Mg-for-Al substitution has been confirmed for several dense hydrous silicates (phase D, Pamato et al. 2015; phase H, Liu et al. 2018; superhydrous Phase B, Kakizawa et al. 2018), Phase Egg has been always reported with the ideal $AlSiO_3(OH)$ stoichiometry. By means of experiments on subsolidus interaction between the lithologies present in subducted slabs — peridotite, mid-ocean ridge basalt (MORB), and sediment —

at 24 GPa and 1400 °C, we synthesized for the first time a Mg-bearing Phase Egg. The new high-pressure phase has been characterized by electron microprobe and single-crystal X-ray diffraction and the results are presented here.

SYNTHESIS

The synthesis was performed in a 2000 ton split-sphere press at Ehime University (Matsuyama, Japan). Eight cubic tungsten carbide anvils with 3 mm truncation edge lengths compressed an 8 mm edge length octahedron of pressure medium of MgO doped with 17 wt% CoO. 4 mm pyrophyllite gaskets sealed the compressed volume and supported the anvil flanks. Heating was provided by a cylindrical $LaCrO_3$ heater, 3.2/2.0 mm in outer/inner diameter and 4 mm in length.

Our experiment (run 3157) combined equal weight of two synthetic mixtures in Re capsules. The bottom half of the capsule held a sediment composition based on the GLOSS (global oceanic subducted sediment) model of Plank and Langmuir (1998) (wt %: 58.55 SiO_2; 0.62 TiO_2; 11.91 Al_2O_3; 5.21 FeO; 0.32 MnO; 2.48 MgO; 5.95 CaO; 2.43 Na_2O; 2.04 K_2O; 0.19 P_2O_5; 3.01 CO_2; 7.29 H_2O). The top half held a garnet lherzolite with modal proportions $Ol_{60}Opx_{16}Cpx_{12}Grt_{12}$ (wt %: 44.99 SiO_2; 3.39 Al_2O_3; 0.5 Cr_2O_3; 11.27 FeO; 37.17 MgO; 2.41 CaO; 0.27 Na_2O). The mixtures were prepared from high-purity reagent-grade oxides (SiO_2, TiO_2, FeO, Cr_2O_3), hydroxides [$Mg(OH)_2$ and $Al(OH)_3$], and carbonates ($CaCO_3$, Na_2CO_3). Temperature during the experiment was controlled by a $W_{97}Re_3$-$W_{75}Re_{25}$ thermocouple, 0.1 mm in diameter. Pressure was calibrated at room temperature using the semiconductor-metal transitions of Bi, ZnS, and GaAs (Irifune et al. 2004). The effect of temperature on pressure was further corrected using the forsterite-wadsleyite and wadsleyite-ringwoodite transitions in Mg_2SiO_4 (Katsura and Ito 1989).

Runs were heated for 4 h and quenched by turning off power to the heater. The capsule was recovered, mounted in epoxy, sectioned, and polished.

Three zones are distinguished after run: peridotite, GLOSS, and the zone of interaction between them (Fig. 1). The latter mostly formed at the expense of the GLOSS zone. Bridgmanite predominates in both peridotite and GLOSS zones. Bridgmanite in the peridotite zone is Cr-bearing, whereas bridgmanite in the GLOSS zone is Ti-bearing and displays higher Al content. The peridotite zone contains minor $CaSiO_3$-perovskite and stishovite. The interaction zone is composed of Al-rich superhydrous phase B, Mg-bearing phase Egg, and minor magnesite. All the phases have been identified by X-ray diffraction.

As is evident from Figure 1, the formation of Al-rich hydrous phases proceeds via peridotite-GLOSS interaction. Although the bulk Al content in the GLOSS part of the sample is high (11.91 wt % Al_2O_3), bridgmanite in the GLOSS zone is Al-depleted (i.e. 7.92 wt % Al_2O_3), because high-Al bridgmanite is not stable under hydrous conditions (Ohira et al. 2014) and decomposes to form high-Al hydrous phases in the reaction zone.

CHEMICAL COMPOSITION

The chemical composition of Mg-bearing Phase Egg was first qualitatively analyzed with energy-dispersive X-ray spectroscopy (EDS). The analyses did not indicate the presence of elements ($Z > 9$) other than Al, Mg, Si and minor Cr and Fe. Quantitative wavelength-dispersive X-ray (WDS) analyses ($n = 4$) were obtained using the same crystal studied by X-ray single-crystal diffraction (see below). A JEOL-JXA 8200 microprobe was operated at 15 kV, 10 nA, and 1 μm beam size, with counting times 20 s on-peak and 10 s for each background position. *Kα* lines for all analyzed elements were referenced to synthetic mineral standards. The crystal is chemically homogeneous within the uncertainty of our measurements (Table 1). The empirical formula (based on 2 filled M-sites per

109 formula unit), assuming all Fe divalent, all Cr as trivalent, and H_2O content calculated from
110 the ideal formula $M^{3+}_{1-x}M^{2+}_{x}SiO_4H_{1+x}$ is $(Al_{0.63}Mg_{0.34}Cr^{3+}_{0.02}Fe^{2+}_{0.01})_{\Sigma=1.00}Si_{1.00}O_4H_{1.35}$,
111 giving $x = 0.35$.
112

113 **X-RAY CRYSTALLOGRAPHY AND STRUCTURE REFINEMENT**

114 A small fragment (15 × 11 × 9 μm in size) of Mg-bearing Phase Egg from run 3157
115 (Fig. 1) was extracted from the polished experimental product under a reflected light
116 microscope and mounted on a 5 μm diameter carbon fiber, which was, in turn, attached to a
117 glass rod. Single-crystal X-ray diffraction intensity data were collected with a Bruker D8
118 Venture Photon 100 CMOS equipped with graphite-monochromatized Mo*K*α radiation
119 operating at 60 kV. The detector-to-crystal distance was 50 mm. Data were collected using
120 ω and φ scan modes, in 0.5° slices, with an exposure time of 75 s per frame. The data were
121 corrected for Lorentz and polarization factors and absorption using the software package
122 *APEX3* (Bruker AXS Inc. 2016). A total of 955 unique reflections was collected. Given the
123 similarity in unit-cell values and space groups, the structure was refined starting from the
124 atomic coordinates reported for the $P2_1/n$ crystal structure of Phase Egg (Schmidt et al.
125 1998) using the program Shelxl-97 (Sheldrick 2008). The unit-cell values are: a =
126 7.2681(8), b = 4.3723(5), c = 7.1229(7) Å, β = 99.123(8)°, V = 223.49(4) Å^3. Vacancies
127 were allowed on the Al and Si sites, estimated using scattering curves for neutral atoms
128 taken from the *International Tables for Crystallography* (Wilson 1992). The mean electron
129 number refined at the *M*1 site (Al site in Phase Egg) was 12.6 e^-, in excellent agreement
130 with that calculated from the microprobe data (12.7 e^-), whereas the mean electron number
131 at the *M*2 site (Si site in Phase Egg) was 14.0 e^-, indicating full occupancy by silicon. The
132 occupancy of only the *M*1 site by Mg was also confirmed by the comparison of bond
133 lengths in the refined structure to the Mg-free structure. At the last stage of refinement the

site occupancy of the *M*1 site was fixed to $Al_{0.65}Mg_{0.35}$ in agreement with the chemical analysis, and the occupancy of the *M*2 site (only Si) was set to unity. At the last stage, with anisotropic displacement parameters for all the atoms, the structure was refined to *R*1 = 0.0166. Hydrogen atoms were not located in the difference Fourier maps. The list of observed and calculated structure factors and the CIF are deposited[1].

RESULTS AND DISCUSSION

The unit-cell parameters of Mg-bearing Phase Egg are only slightly influenced by the entry of Mg into the structure. We observed a general expansion of the unit cell, mainly related to the increase of the *c* parameter (by 2.4%) from pure $AlSiO_3(OH)$ (Schmidt et al. 1998), although the increase is quite isotropic.

The assignment of Mg to the *M*1 site (Al site) of Phase Egg is required both to account for the electron density at that site and, more importantly, to justify the increase of the bond distances relative to pure $AlSiO_3(OH)$ (Schmidt et al. 1998). The mean bond distance of the Al site of Phase Egg increases with the entry of Mg from 1.890 Å to 1.928 Å. The mean octahedral Si-O distance increases only slightly with the general incorporation of Mg in the structure, from 1.814 and 1.840 Å. Interestingly, the anomalous (5+1)-coordination of silicon observed for Phase Egg (Schmidt et al. 1998) is confirmed, and even more pronounced, in Mg-bearing Phase Egg. The ^{longest}[Si-O] – ^{V}[<Si-O>] parameter, defined as the difference between the longest Si-O distance and the average values of the other 5 similar Si-O distance, is 0.302 Å in $AlSiO_3(OH)$ and increases to 0.351 Å in the crystal studied in the present study. Interestingly, the Mg-for-Al substitution induces a slight distortion of the Al-octahedral site, quantified by an increase of the octahedral angle

[1] For a copy of the list of observed and calculated structure factors and CIF, document item AMxxxxx, contact the Business Office of the Mineralogical Society of America (see inside front cover of recent issue) for price information. Deposit items may also be available on the American Mineralogist web site at http://www.minsocam.org.

variance σ^2 (Robinson et al. 1971) from 43.80 in pure $AlSiO_3(OH)$ (Schmidt et al. 1998) to 49.20 in Mg-bearing Phase Egg. On the other hand, the Si-octahedron is somewhat more regular ($\sigma^2 = 40.92$) than that in pure Al-Egg ($\sigma^2 = 42.35$).

The crystal structure consists of edge-shared Si-octahedra, linked to an $(Al,Mg)_2O_{10}$ dimer. As pointed out by Schmidt et al. (1998), the way these units are linked to form the structure resembles that of stishovite, wherein edge-linked octahedra form columns of corner-linked octahedra. H atoms in Phase Egg are in the cavities between the columns. Bond valence sums (BVS), calculated according to the values by Brese and O'Keeffe (1991), show low values for all the oxygen atoms (Table 2). O3 and O4 were already identified as acceptor and donor of a hydrogen atom in Phase Egg. In the present crystal, the minor undersaturation shown by O1 and O2 could indicate the presence of a second hydrogen-bonding system, which is only partially represented (estimated occupancy for the additional H atom = 0.35 atoms per formula unit). There are not O1–O2 short distances that are not polyhedral edges in the structure. The only plausible O-O short distances for the second hydrogen-bonding system are represented by either O1–O1 [3.124(2) Å] or O2–O2 [4.373(3) Å], both in the cavities between the columns of octahedra. Although such bonds are long and not ideal, they could link the second H, which is only partially present. Otherwise, the second H could be statistically distributed between the two positions. We analyze Mg-bearing Phase H by Fourier-Transform Infrared spectroscopy to shed light on the OH environments with two different equipments (both at the University of Padua and at the Caltech), but, unfortunately, the results were dramatically affected by organic contamination and we could not state with confidence if the bands we were focusing on were due to hydrogen in the structure.

Komatsu et al. (2006) showed that the crystal structure of pure δ-AlOOH is non-centrosymmetric, space group $P2_1nm$. The entry of Mg and Si substituting for Al (even in

very low amounts) was observed to provoke the $P2_1nm \rightarrow Pnnm$ transition (Komatsu et al. 2011), which was later shown to be also the space group of pure $MgSiH_2O_4$, known as Phase H (Bindi et al. 2014). Interestingly, we did not observe any structural change from pure $AlSiO_3(OH)$ to $Al_{1-x}Mg_xSiO_4H_{1+x}$ with $x = 0.35$. Thus, it seems that the disorder at the octahedral sites induced by cations with different valence states (i.e., Mg^{2+}, Al^{3+} and Si^{4+}) does not provoke any fluctuation of the hydrogen positions. This observation implies that Phase Egg should be able to incorporate, without any phase transition, even greater amounts of hydrogen than that documented in this study. In particular, solid solution may extend all the way the ideal endmember $MgSiH_2O_4$, which would represent a polymorph of Phase H.

IMPLICATIONS

Experimental data suggest that hydrous and CO_2-bearing sediments (e.g., pelites) can be transported deep into the mantle without melting (Poli et al. 2009; Wu et al. 2009). Interaction between model sediment and peridotite has been previously studied using a multi-anvil apparatus at 7.5–12 GPa and 900–1400 °C (Bulatov et al. 2014), demonstrating that subducted oceanic crust could deliver significant contents of water to a depth greater than 300 km. The stability of hydrous phases beyond the base of the transition zone at 670 km is controversial. Recent studies (e.g., Kakizawa et al. 2018) have shown that water could be transported to the lower mantle by the dense hydrous magnesium silicates superhydrous phase B and phase D in the cold slab. Their stability expands to higher temperatures with incorporation of Al_2O_3. Phase Egg (Eggleton et al. 1978) is stable in the transition zone and in the lower mantle as well, and its likely discovery as an inclusion in diamond (Wirth et al. 2007) and now the fact that it forms by peridotite-sediment reaction and can host appreciable amounts of Mg provide direct mineralogical support for a stable

207 solid host for water at transition zone pressures in compositions where ringwoodite is
208 absent.
209
210 **ACKNOWLEDGMENTS**
211 Paul Asimow, George Rossman and Fabrizio Nestola are thanked for the efforts to
212 obtain an IR/Raman spectrum of Mg-bearing Phase Egg. The manuscript took advantage
213 from the revision of three anonymous reviewers. Zhicheng Jing is gratefully acknowledged
214 for the efficient handling of the manuscript. The research was supported by "progetto di
215 Ateneo 2016, University of Firenze" to LB and by the Russian Science Foundation, project
216 no. 17-17-01169 to AB, AB, and ES.
217
218 **REFERENCES CITED**
219 Bindi, L., Nishi, M., Tsuchiya, J., and Irifune, T. (2014) Crystal chemistry of dense hydrous
220 magnesium silicates: The structure of Phase H, $MgSiH_2O_4$ synthesized at 45 GPa and
221 1000 °C. American Mineralogist, 99, 1802–1805.
222 Brese, N.E., and O'Keeffe, M. (1991) Bond-valence parameters for solids. Acta
223 Crystallographica, B47, 192–197.
224 Bruker (2016) *APEX3*, *SAINT* and *SADABS*. Bruker AXS Inc., Madison, Wisconsin, USA.
225 Bulatov, V.K., Brey, G.P., Girnis, A.V., Gerdes, A., and Höfer, H.E. (2014) Carbonated
226 sediment–peridotite interaction and melting at 7.5–12 GPa. Lithos, 200-201, 368–
227 385.
228 Eggleton, R.A., Boland, N.J., and Ringwood, A.E. (1978) High pressure synthesis of a new
229 aluminum silicate: $Al_5Si_5O_{17}(OH)$. Geochemical Journal, 12, 191–194.
230 Frost, D.J., and Fei, Y. (1998) Stability of phase D at high pressure and high temperature.
231 Journal of Geophysical Research, 103, 7463–7474.

Fukuyama, K., Ohtani, E., Shibazaki, Y., Kagi, H., and Suzuki, A. (2017) Stability field of Phase Egg, $AlSiO_3OH$ at high pressure and high temperature: possible water reservoir in mantle transition zone. Journal of Mineralogical and Petrological Sciences, 112, 31–35.

Irifune, T., Kurio, A., Sakamoto, S., Inoue, T., Sumiya. H., and Funakoshi, K. (2004) Formation of pure polycrystalline diamond by direct conversion of graphite at high pressure and high temperature. Physics of the Earth and Planetary Interiors, 143-144, 593–600.

Kakizawa, S., Inoue, T., Nakano, H., Kuroda, M., Sakamoto, N., and Yurimoto, H. (2018) Stability of Al-bearing superhydrous phase B at the mantle transition zone and the uppermost lower mantle. American Mineralogist, 103, 1221–1227.

Kaminsky, F. (2012) Mineralogy of the lower mantle: A review of 'super-deep' mineral inclusions in diamond. Earth-Science Reviews, 110, 127–147.

Katsura, T., and Ito, E. (1989) The system Mg_2SiO_4-Fe_2SiO_4 at high pressure and temperatures: Precise determination of stabilities of olivine, modified spinel, and spinel. Journal of Geophysical Research, 94, 15663–15670.

Komatsu, K., Kuribayashi, T., Sano, A., Ohtani, E., and Kudoh, Y. (2006) Redetermination of the high-pressure modification of AlOOH from single-crystal synchrotron data. Acta Crystallographica, E62, i216–i218.

Komatsu, K., Sano-Furukawa, A., and Kagi, H. (2011) Effects of Mg and Si ions on the symmetry of δ-AlOOH. Physics and Chemistry of Minerals, 38, 727–733.

Liu, G., Liu, L., Yang, L., Yi, L., Li, Y., Liu, H., Gao, Y., Zhuang, C., and Li, S. (2018) Crystal structure and elasticity of Al-bearing phase H under high pressure. AIP Advances 8, 055219.

Nishi, M., Irifune, T., Tsuchiya, J., Tange, Y., Nishihara, Y., Fujino, K., and Higo, Y. (2014) Stability of hydrous silicate at high pressures and water transport to the deep lower mantle. Nature Geoscience, 7, 224–227.

Ohira, I., Ohtani, E., Sakai, T., Miyahara, M., Hirao, N., Ohishi, Y., and Nishijima, M. (2014) Stability of a hydrous-phase, AlOOH-$MgSiO_2(OH)_2$, and a mechanism for water transport into the base of lower mantle. Earth and Planetary Science Letters, 401, 12–17.

Ohtani, E., Mizobata, H., and Yurimoto, H. (2000) Stability of dense magnesium silicate phases in the systems Mg_2SiO_4-H_2O and $MgSiO_3$-H_2O at pressures up to 27 GPa. Physics and Chemistry of Minerals, 27, 533–544.

Pamato, M.G., Myhill, R., Boffa-Ballaran, T., Frost, D.J., Heidelbach, F., and Miyajima, N. (2015) Lower-mantle water reservoir implied by the extreme stability of a hydrous aluminosilicate. Nature Geoscience, 8, 75–79.

Pearson, D.G., Brenker, F.E., Nestola, F., McNeill, J., Nasdala, L., Hutchison, M.T., Matveev, S., Mather, K., Silversmit, G., Schmitz, S., Vekemans, B., and Vincze, L. (2014) Hydrous mantle transition zone indicated by ringwoodite included within diamond. Nature, 507, 221–224.

Plank, T., and Langmuir, C.H. (1998) The chemical composition of subducting sediment and its consequences for the crust and mantle. Chemical Geology, 145, 325–394.

Poli, S., Franzolin, E., Fumagalli, P., and Crottini, A. (2009) The transport of carbon and hydrogen in subducted oceanic crust: an experimental study to 5 GPa. Earth and Planetary Science Letters, 278, 350–360.

Robinson, K., Gibbs, G.V., and Ribbe, P.H. (1971) Quadratic elongation: a quantitative measure of distortion in coordination polyhedra. Science, 172, 567–570.

280 Schmidt, M.W., Finger, L.W., Angel, R.J., and Dinnebier, R.E. (1998) Synthesis, crystal
281 structure, and phase relations of $AlSiO_3OH$, a high-pressure hydrous phase. American
282 Mineralogist, 83, 881–888.
283 Sheldrick, G.M. (2008) A short history of SHELX. Acta Crystallographica, A64, 112–122.
284 Shieh, S.R., Mao, H-K., Hemley, R.J., and Ming, L.C. (1998) Decomposition of phase D in
285 the lower mantle and the fate of dense hydrous silicates in subducting slabs. Earth and
286 Planetary Science Letters, 159, 13–23.
287 Smith, E.M., Shirey, S.B., Nestola, F., Bullock, E.S., Wang, J., Richardson, S.H., and
288 Wang, W. (2016) Large gem diamonds from metallic liquid in Earth's deep mantle.
289 Science, 354, 1403–1405.
290 Smith, E.M., Shirey, S.B., Richardson, S.H., Nestola, F., Bullock, E.S., Wang, J., and
291 Wang, W. (2018) Blue boron-bearing diamonds from Earth's lower mantle. Nature,
292 560, 84–87.
293 Tsuchiya, J. (2013) First principles prediction of a new high-pressure phase of dense
294 hydrous magnesium silicates in the lower mantle. Geophysical Research Letters, 40,
295 4570–4573.
296 Wilson, A.J.C., Ed. (1992) *International Tables for Crystallography*, Volume C:
297 Mathematical, physical and chemical tables. Kluwer Academic, Dordrecht, NL
298 Wirth, R., Vollmer, C., Brenker, F., Matsyuk, S., and Kaminsky, F. (2007) Inclusions of
299 nanocrystalline hydrous aluminium silicate "Phase Egg" in superdeep diamonds from
300 Juina (Mato Grosso State, Brazil). Earth and Planetary Science Letters, 259, 384–399.
301 Wu, Y., Fei, Y., Jin, Z., and Liu, X. (2009) The fate of subducted upper continental crust:
302 An experimental study. Earth and Planetary Science Letters, 282, 275–284.

303 Xue, X., Kanzaki, M., Fukui, H., Ito, E., and Hashimoto, T. (2006) Cation order and
304 hydrogen bonding of high-pressure phases in the Al_2O_3-SiO_2-H2O system: An NMR
305 and Raman study. American Mineralogist, 91, 850–861.

306

307

308

309 **FIGURE CAPTIONS**

310 FIGURE 1. SEM-BSE images the run 3157 (P = 24 GPa, T = 1400 °C). The bottom image is a
311 blow-up of the region highlighted with the dashed red rectangle in the top image.
312 Mg-bearing Phase Egg (Mg-Egg) is associated with bridgmanite (Brd),
313 superhydrous Phase B (SuB), stishovite (Sti), Ca-perovskite (Ca-Pv), and
314 magnesite (Mgs). CamScan electronic microscope MV2300.

315 Figure 2. The crystal structure of Mg-bearing Phase Egg down the [100] axis. (Al,Mg)- and
316 Si-octahedra are drawn in light orange and dark green, respectively.

317

TABLE 1. Electron microprobe analyses (wt% of oxides) of the crystal used for the structural study together with the atomic ratios calculated on the basis of two cations.

SiO_2	49.76
Al_2O_3	26.66
Cr_2O_3	1.32
MgO	11.13
FeO	0.54
total	89.41
H_2O*	10.20
total	99.61
Si	1.003
Al	0.633
Cr	0.021
Mg	0.334
Fe	0.009
total	2.000

*H_2O calculated from the ideal formula $M^{3+}_{1-x}M^{2+}_{x}SiO_4H_{1+x}$ with x = 0.35. Iron and Cr were assumed to be divalent and trivalent, respectively.

TABLE 2. Bond-valence (*v.u.*) arrangement for the Mg-bearing Phase Egg.

	*M*1	*M*2	Σ O
	$Al_{0.63}Mg_{0.34}Cr_{0.02}Fe_{0.01}$	$Si_{1.00}$	
O1	0.517	0.658	1.833
		0.658	
O2	0.553	0.709	1.901
		0.639	
O3	0.422	0.756	1.591
	0.413		
O4	0.508	0.266	1.185
	0.411		
	2.824	3.686	

Note: calculated from the bond-valence curves of Brese and O'Keeffe (1991)

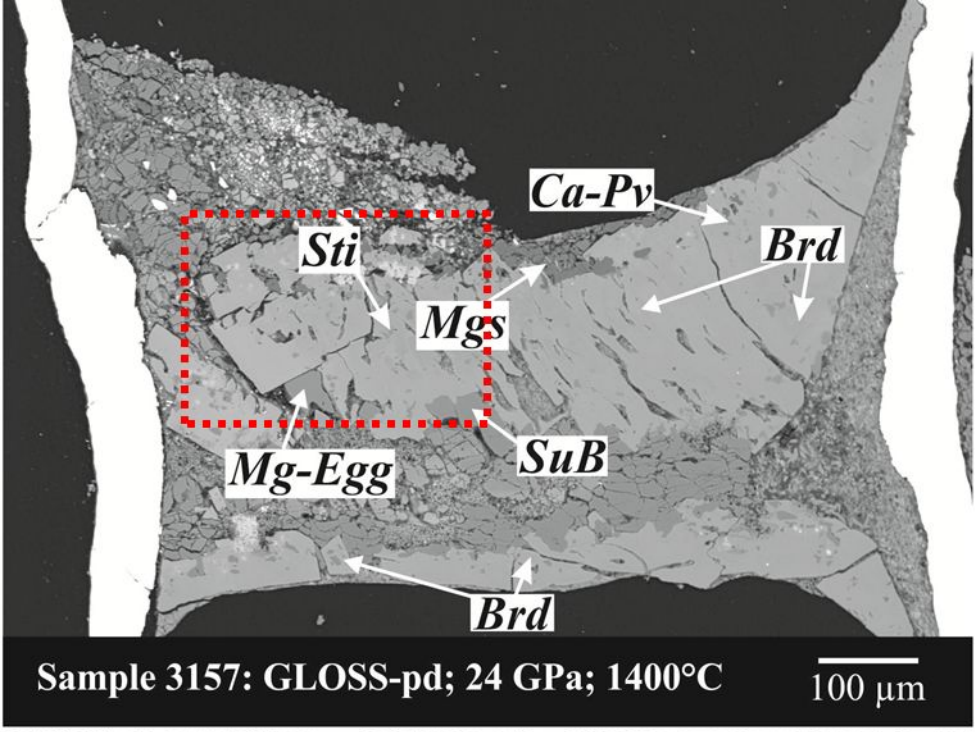
Ca-Pv
Sti
Brd
Mgs
Mg-Egg
SuB
Brd
Sample 3157: GLOSS-pd; 24 GPa; 1400°C
100 µm

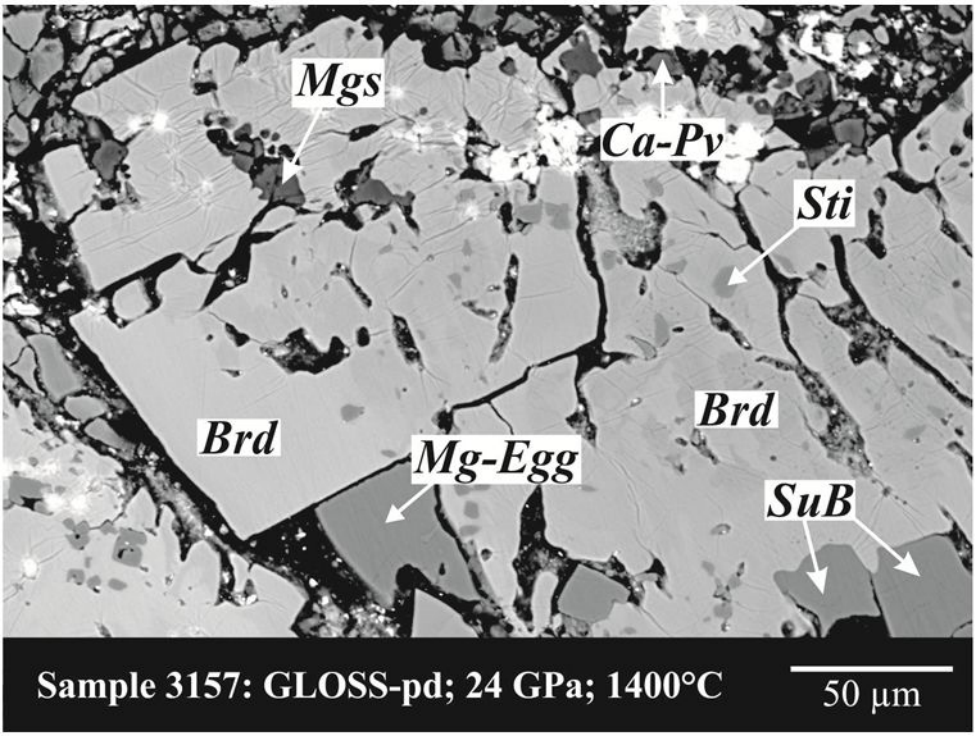
Mgs
Ca-Pv
Sti
Brd
Brd
Mg-Egg
SuB
Sample 3157: GLOSS-pd; 24 GPa; 1400°C
50 µm

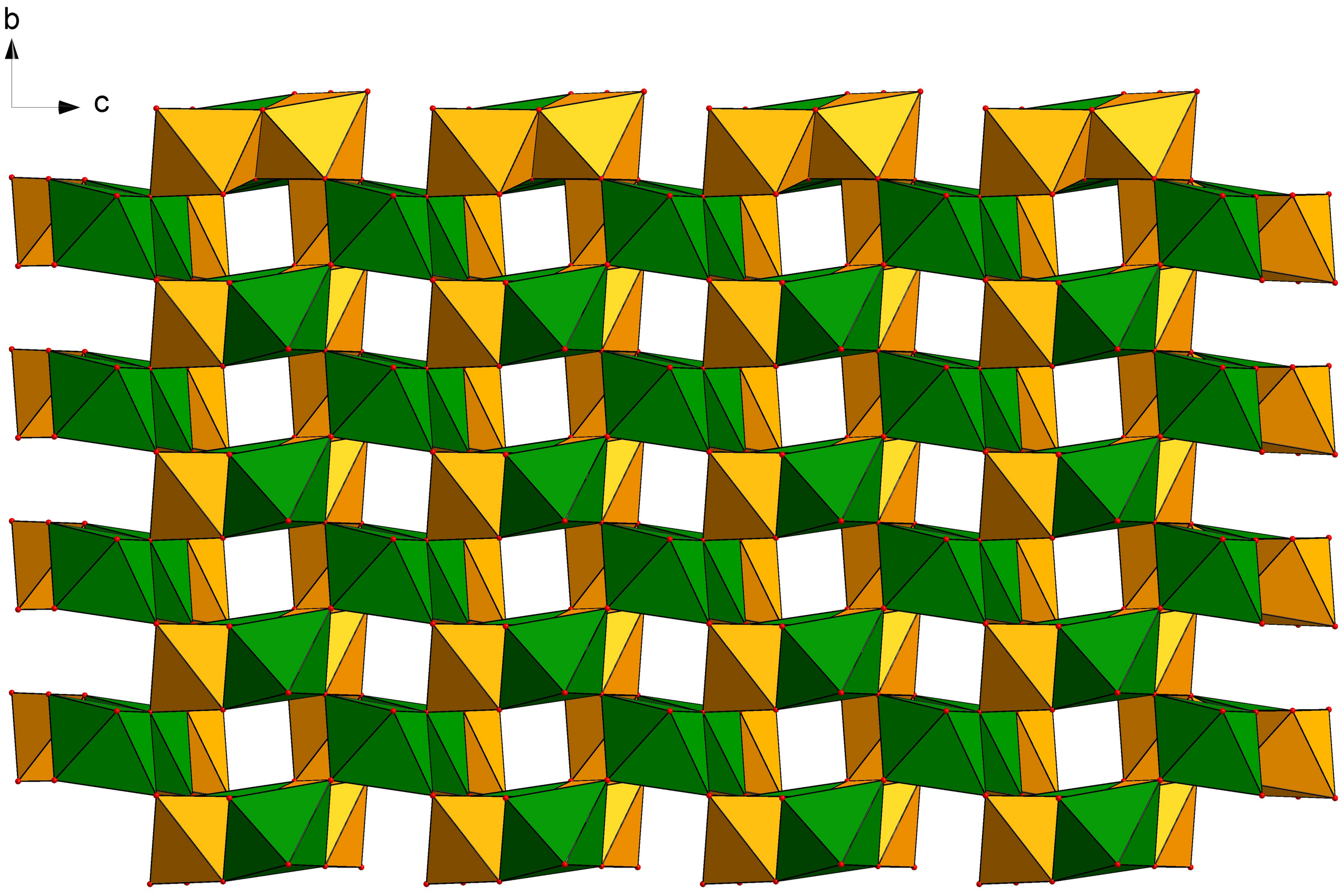
b
c